© 2018. Published by The Company of Biologists Ltd | Development (2018) 145, dev165852. doi:10.1242/dev.165852

TECHNIQUES AND RESOURCES

RESEARCH REPORT

ROSA26 reporter mouse lines and image analyses reveal distinct region-specific cell behaviors in the visceral endoderm

Takaya Abe[1,2,3,4,*], Natsumaro Kutsuna[5,6], Hiroshi Kiyonari[1,2,3,4], Yasuhide Furuta[1,2,3,4] and Toshihiko Fujimori[2,4,7,8,*]

ABSTRACT

The early post-implantation mouse embryo changes dramatically in both size and shape. These morphological changes are based on characteristic cellular behaviors, including cell growth and allocation. To perform clonal analysis, we established a Cre/*loxP*-based reporter mouse line, *R26R-ManGeKyou*, that enables clonal labeling with multiple colors. We also developed a novel ImageJ plugin, LP-Clonal, for quantitative measurement of the tilt angle of clonal cluster shape, enabling identification of the direction of cluster expansion. We carried out long-term and short-term lineage tracking. We also performed time-lapse imaging to characterize cellular behaviors using *R26-PHA7-EGFP* and *R26R-EGFP*. These images were subjected to quantitative image analyses. We found that the proximal visceral endoderm overlying the extra-embryonic ectoderm shows coherent cell growth in a proximal-anterior to distal-posterior direction. We also observed that directional cell migration is coupled with cell elongation in the anterior region. Our observations suggest that the behaviors of visceral endoderm cells vary between regions during peri-implantation stages.

KEY WORDS: Mouse embryogenesis, Cell lineage, Cell migration, Visceral endoderm, ROSA26 reporter mouse lines

INTRODUCTION

Rodents exhibit a transient structure called the egg cylinder after implantation (Beddington and Robertson, 1999; Rossant and Tam, 2009; Srinivas, 2006; Tam and Loebel, 2007). Visceral endoderm (VE) cells in the distal tip or distal visceral endoderm (DVE) (Takaoka et al., 2011) migrate to the future anterior side and become the anterior visceral endoderm (AVE) by embryonic day (E) 5.5 (Srinivas et al., 2004). The anterior-posterior (A-P) axis is specified in a process called original AVE migration. Subsequently, from E6.0 onwards, newly induced AVE cells migrate to the anterior side in a process called secondary AVE migration. Meanwhile, the original AVE cells in the anterior side move to the lateral side (Takaoka et al., 2011; Trichas et al., 2011). Divergent cell movements associated with A-P axis formation were previously observed (Srinivas, 2006; Srinivas et al., 2004). However, the general behaviors of VE cells are not well studied, and regional differences in cell behavior are not clearly understood.

It is difficult to trace cell lineages over a long period during peri-implantation stages using classical techniques based on either cell labeling with dyes (Gardner and Cockroft, 1998; Lawson and Pedersen, 1987) or mRNA injection (Weber et al., 1999) because of rapid dilution. To overcome this problem, genetic lineage labeling induced by either stochastic DNA recombination (Tzouanacou et al., 2009) or the Cre/*loxP* system (Fujimori et al., 2003) were employed. Lineage-tracing experiments have been performed using a multicolor lineage-tracing reporter mouse based on the Brainbow construct in neurons, small intestinal stem cells, and pre-implantation embryos (Livet et al., 2007; Snippert et al., 2010; Tabansky et al., 2013). Other combinatorial multicolor tracing systems have been expanded to other model organisms (Weissman and Pan, 2015), but most analyses of clonal clusters have been limited to qualitative observations. Some studies included quantitative statistical measurements of the spatial distributions of labeled cells (Ghigo et al., 2013). However, quantitative image analysis aimed at understanding the morphological changes in clonal cluster shapes remains very limited.

In this study, we established a multicolored lineage-tracing reporter mouse *R26R-ManGeKyou* (*R26R-MGK*) that allows us to trace the individual lineages of multiple cells using fluorescent proteins expressed under endogenous *ROSA26* promoter (Soriano, 1999). We devised this new system in part because the Brainbow cassette in *R26R-Confetti* is expressed by a strong promoter, *CAG*, which is silenced in some tissues, especially the extra-embryonic (ExEm) VE (Abe et al., 2013b; Griswold et al., 2011). Furthermore, we developed a novel plugin for ImageJ for quantification of cell cluster shapes. In combination with time-lapse imaging using other reporter mouse lines and another quantitative image analysis system, we uncovered region-specific differential cell behaviors in the VE in early post-implantation embryos.

RESULTS

ManGeKyou multicolor reporter mouse line establishment

To analyze multiple cell lineages simultaneously in a single embryo, we generated a reporter mouse line, named *R26R-ManGeKyou* (*R26R-MGK*) (Fig. 1A). We inserted a construct comprising a splicing acceptor, a *loxP*-flanked *STOP* cassette (Soriano, 1999; Srinivas et al., 2001), and cDNAs encoding three different fluorescent proteins preceded by modified *loxP* sequences (Lee and Saito, 1998). In this configuration, recombination can continue to excise the *lox*-flanked cassette as long as Cre protein persists until the *lox2272*-flanked sequences are removed. We generated *R26R-MGK* embryonic stem cells (ESC) lines by gene

[1]Animal Resource Development, RIKEN Center for Biosystems Dynamics Research, 2-2-3 Minatojima Minami-machi, Chuou-ku, Kobe 650-0047, Japan. [2]Genetic Engineering, RIKEN Center for Biosystems Dynamics Research, 2-2-3 Minatojima Minami-machi, Chuou-ku, Kobe 650-0047, Japan. [3]Animal Resource Development Unit, RIKEN Center for Life Science Technologies, 2-2-3 Minatojima Minami-machi, Chuou-ku, Kobe 650-0047, Japan. [4]Genetic Engineering Team, RIKEN Center for Life Science Technologies, 2-2-3 Minatojima Minami-machi, Chuou-ku, Kobe 650-0047, Japan. [5]Department of Integrated Biosciences, Graduate School of Frontier Science, The University of Tokyo, Kashiwa 277-8562, Japan. [6]Research & Development Department, LPixel Inc., TechLab 6F, Otemachi Building, 1-6-1, Otemachi, Chiyoda-ku, Tokyo, 100-0004, Japan. [7]Division of Embryology, National Institute for Basic Biology (NIBB), Okazaki 444-8787, Japan. [8]Department of Basic Biology, School of Life Science, Sokendai 444-8787, Japan.

*Authors for correspondence (takaya.abe@riken.jp; fujimori@nibb.ac.jp)

T.A., 0000-0001-5885-4875; T.F., 0000-0001-5200-4634

Received 21 March 2018; Accepted 8 October 2018

Development (2018) 145, dev165852. doi:10.1242/dev.165852

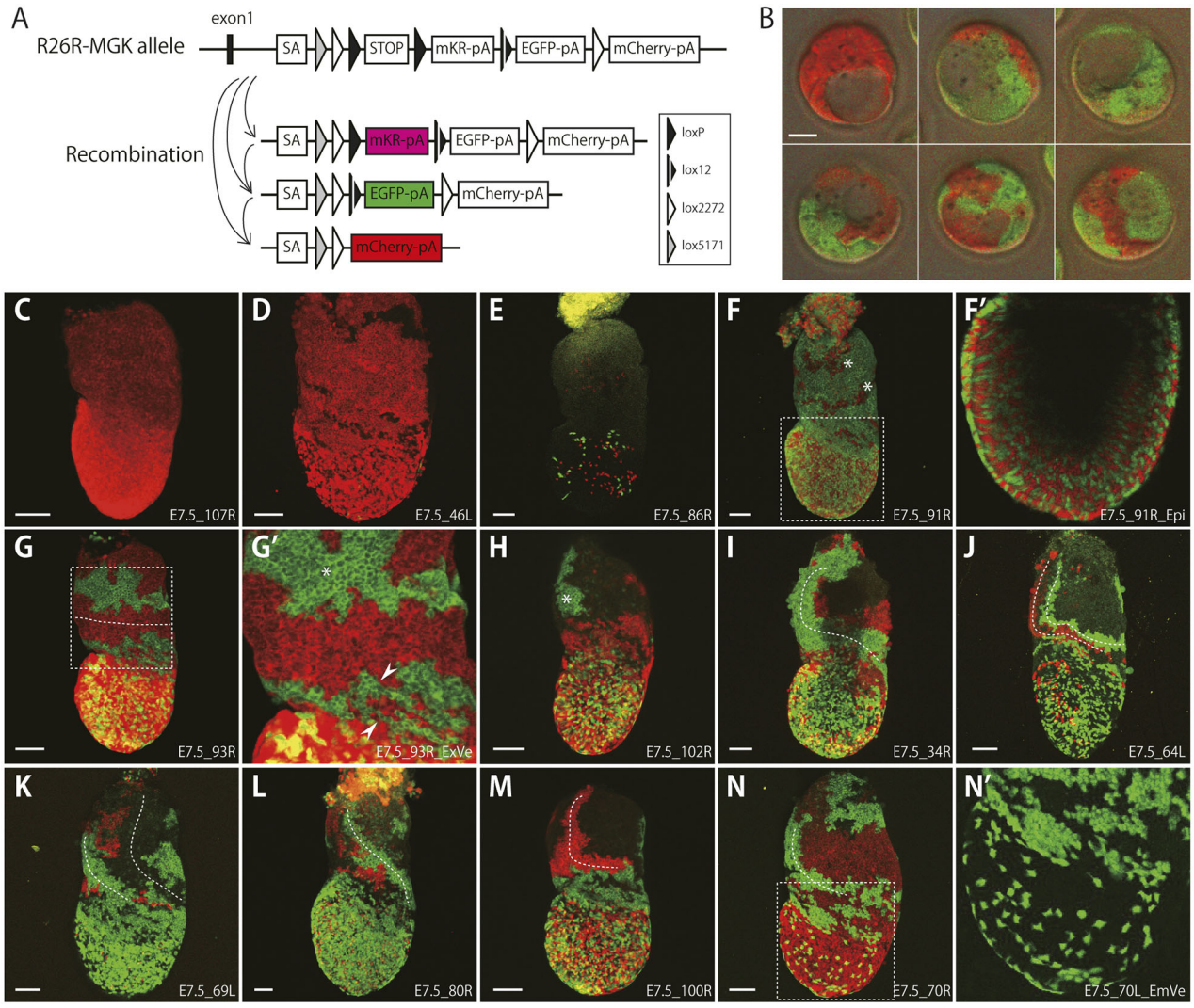

Fig. 1. Cre recombination in *R26R-ManGeKyou* embryos. (A) Cre/*lox* recombination at the *R26R-MGK* allele, showing prospective alleles after recombination. (B-N) *EIIaCre*/*R26R-MGK* embryos expressing EGFP or mCherry. (B) Slice images of blastocysts. (C-N) *z*-stack images of E7.5 embryos. Anterior is to the left. F′, G′ and N′ are enlarged views of boxes shown in F,G and N, respectively. Asterisks indicate coherent patches of cells, arrowheads indicate cell clusters distributed obliquely, and dotted lines indicate cell clusters formed in either vertical or horizontal orientation. Green and red indicate EGFP and mCherry, respectively. Scale bars: 25 µm (B); 100 µm (C-N).

targeting, and no fluorescent proteins were expressed before Cre recombination. After *in vitro* recombination, the ESC colonies either exhibited EGFP or mCherry fluorescence, or remained non-fluorescent. Furthermore, we verified the switch from EGFP to mCherry expression visually (Fig. S1A,B), which indicates stepwise fluorescence switching. For unknown reasons, no colonies expressing mKeima-Red were observed.

We subsequently established the *R26R-MGK* mouse lines. Fluorescence was undetectable before Cre recombination. To test whether excision can occur *in vivo*, *R26R-MGK* mice were crossed with *R26CreER* mice (Badea et al., 2003). Distinct EGFP and mCherry fluorescence showed either salt-and-pepper patterns or some small clusters in various tissues (Fig. S1C-K). Keima-Red signal was barely detectable in these E10.5 embryos, just as in ESCs.

Post-implantation lineages of blastomere descendants

We used *EIIaCre* transgenic mice (Lakso et al., 1996), in which Cre activity has been shown to be random and ceases before implantation (Holzenberger et al., 2000), resulting in mosaic Cre/*loxP* excision. To confirm the time window of recombination, homozygous *EIIaCre* females were crossed with *R26R-MGK* males, and two-cell-stage embryos were isolated for time-lapse imaging (Abe et al., 2013a). One embryo out of the six we examined expressed a single color, whereas the other five embryos carried three cell types that expressed either no fluorescence, EGFP, or mCherry (Fig. 1B). Fluorescence signals became detectable between the four- and eight-cell stages, and signal intensities increased during observation (Movie 1). These results indicate that Cre was active before implantation, and that *EIIaCre* was effective at inducing random and partial Cre/*lox* excision for mosaic cell labeling in *R26R-MGK* embryos.

Next, we collected E7.5 *EIIaCre/R26R-MGK* embryos to characterize the distribution of fluorescent cells. Sixty embryos were collected, and lateral views images were acquired (Fig. 1C-N′, Fig. S2). In five embryos, only mCherry signals were observed in most of the cells (Fig. 1C); two other embryos showed mosaic mCherry patterns (Fig. 1D); in 12 other embryos, fluorescence-positive cells were present only in the embryonic region or in the

Development (2018) 145, dev165852. doi:10.1242/dev.165852

epiblast (Fig. 1E); and the remainder showed widespread and distinct EGFP and mCherry signals (Fig. 1F-N′).

Labeled cells were distributed in salt-and-pepper patterns in the epiblast (Fig. 1F′). By contrast, various distribution patterns were observed in the VE layer, depending on the region. In the ExEm region, cells with the same color showed various coherent clusters. Some clusters elongated along the proximal-distal (P-D) axis whereas others elongated perpendicular to the P-D axis (Fig. 1F,G′,H, white asterisks). Moreover, twisted forms of clusters were observed in 19 images. In these embryos, cell clusters elongated within the VE from proximal to distal along the anterior edge of the ExEm region and ran along the border between the embryonic (Em) and ExEm regions from anterior to posterior (Fig. 1I-N, white dotted lines). Cell clusters near the border between ExEm and Em regions were elongated obliquely from anterior-proximal to posterior-distal orientations (Fig. 1G′, white arrowheads). VE cells in the lateral region overlying the epiblast, however, did not form any coherent patches and clusters with the same color. Moreover, these cells exhibited filopodia-like protrusions (Fig. 1N′).

Quantitative shape analysis of VE cell clusters

In order to characterize the cluster shapes of VE cells and determine if there are trends between embryos quantitatively, we developed LP-Clonal, a plugin for ImageJ that can quantify the tilt angles of the shapes of cell clusters. The developmental stages of embryos varied slightly even within the same litter. Hence, we decided to define a standard shape using the average shape of embryos. The initial normalizing procedure involves proportional enlargement or reduction of each image to fit the standard shape required for image analysis (Fig. 2A,A′). Binary images were generated from the resized image (Fig. 2A″, Fig. S3), and divided into 100×100 pixel sections for analysis. The angles of elongated cell cluster shapes were computed from the normalized binary images, and the acquired angles were represented as an elliptical diagram (Fig. 2A‴). The average values of the angle in each ellipse position were further calculated from multiple embryo images, and depicted as a cumulative diagram (Fig. 2B).

We applied this analysis scheme to 87 images (GFP, mCherry, left and/or right) derived from 32 embryos, excluding images in which fluorescence signals were observed only in the Em region and those in which a large single cluster with red fluorescence was observed in the ExEm region. Cell clusters in the ExEm region were usually large, and showed some common patterns in cluster shapes. We focused on the areas indicated with colored boxes in the ExEm region by arbitrarily subdividing this region into nine compartments (Fig. 2B). Scatter plots show the mean value of the ellipse angle at each position, and lines indicate average values of angles in the corresponding colored boxes (Fig. 2C). In the proximal part of the ExEm region (row I), ellipses were oriented vertically in the anterior compartment (red boxed area) with the average angle value closer to 90° compared with that of the posterior regions (Fig. 2C, row I). By contrast, in more distal ExEm regions (row II), ellipses showed horizontal alignment regardless of A-P position. Moreover, in the most distal ExEm regions (row III), ellipses near the boundary between the ExEm and Em regions appeared to incline from anterior-proximal to posterior-distal orientation.

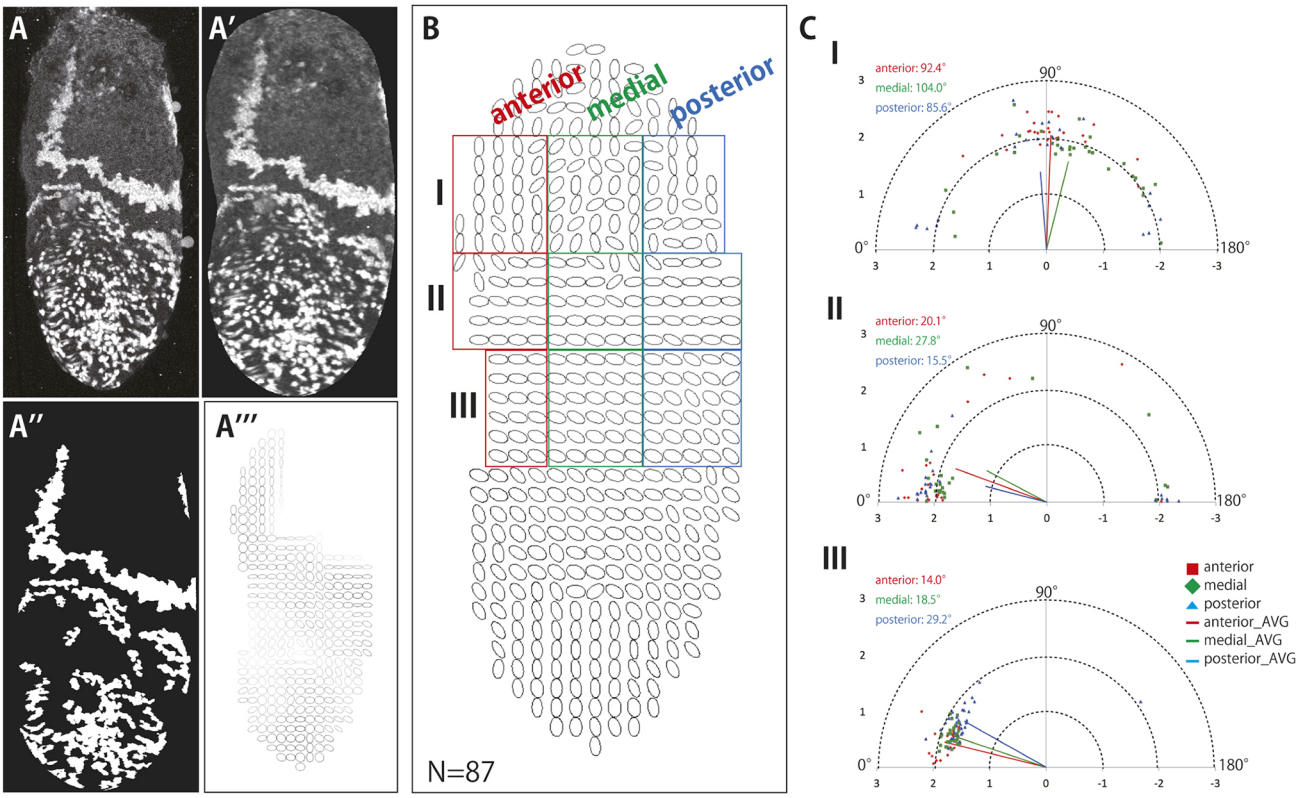

Fig. 2. Quantitative analysis of cluster shapes. (A) Single channel *z*-stack lateral image of an E7.5 *EllaCre*/*R26R-MGK* embryo. Anterior is to the left. (A′) Shape-normalized image of the embryo shown in A. (A″) Binary image of A′. (A‴) Diagram generated by LP-Clonal plugin. (B) Representative diagram of average values from 87 images. The VE layer in the ExEm area is subdivided into nine compartments, shown as colored boxes. (C) Scatter plots of ellipse angles in each of the colored boxes indicated in B. In B and C, red, green and blue indicate anterior, medial and posterior regions, respectively; each is further compartmentalized proximodistally into I, II and III. Diameter of semicircular graphs represents ellipticity and reliability after quantification with LP-Clonal.

Development (2018) 145, dev165852. doi:10.1242/dev.165852

Clonal analyses during the gastrulation stage following pulse labeling of cells

To follow cell behaviors over a shorter period, we induced Cre recombination in *R26CreER/R26R-MGK* embryos at E5.5 using tamoxifen and collected them subsequently at E7.5 (Fig. 3A, Fig. S4). Twenty-three embryos were collected and imaged. Of the images collected, 31 showed various coherent patches in the VE layer. We measured the angle between the maximum caliper and a line parallel to the *x*-axis of each image (FeretAngle) and the area of each cell patch (Area) using an ImageJ plugin, Shape Descriptor Maps (BioVoxxel Toolbox) (Schäfer et al., 2016) (Fig. 3A′,A″). We analyzed 66 cell patches in total, each comprising 2-26 cells (8.0 cells on average) (Fig. S5). In the proximal portion (Fig. 3A, region I), patches showed a tendency to extend vertically, an average of 77.6° across 23 cell patches (Fig. 3B). Those in the middle portion (Fig. 3A, region II) showed oblique orientations, with an average of 61.8° across 43 cell patches (Fig. 3B). These tendencies were consistent with our cluster-shape analysis (Fig. 2). Differences in cell behaviors between ExEm and Em regions were also observed during time-lapse observation of random cell labeling with EGFP (Fig. S6, Movies 2, 3). Sister cells maintained their close association even after VE cell division in proximal regions.

Analyses of changes in cell shape and relative position of cells with related cellular behaviors

We investigated the apical cell shape of the VE to understand how the shape and relative positions of cells change. We performed time-lapse recording of *R26-PHA7-EGFP* embryos, which express the chimeric protein PHA7-EGFP, a fusion of Plekha7, an adherens junction component protein, to EGFP (Meng et al., 2008; Shioi et al., 2017). We observed collective migration by about 20 closely associated cells from the distal tip of the embryo to the anterior region from E6.25 to E6.4 (Fig. 4D,G, Movies 4, 7, 8, 9) (n=4). The apical surface of these cells shrank just before migration, and the cells migrated collectively thereafter to an anterior position in the embryonic region. We observed junctional remodeling when cells approached the border between the ExEm and Em (Fig. S7). This migration pattern was associated with the characteristic movement of cells along the lateral side near the border in the posterior direction, resulting in elongated shapes on the anterior side near the border (Fig. 4C,E,H,I, Movie 5). These cells did not cross the border between the ExEm and Em regions. VE cells in the ExEm region did not show active movements (Fig. 4F, Movie 6), instead maintaining their positions. EmVE cells in the posterior-lateral and posterior-distal planes adjacent to the AVE cells did not move actively during migration, whereas the surface area expanded, providing a mechanism to immediately fill the space that was previously occupied by anterior EmVE cells that had migrated.

We observed apparent region-specific differences in apical cell shapes, and quantified those shapes (Fig. 4A,A′). We focused on the area (Fig. 4B,B′) and the ratio between the maximum and minimum diameters (aspect ratio) (Fig. 4C,C′). The average area of VE cells at the anterior Em region (III) was the smallest (Fig. 4B′, region III), and the distal Em region (IV) was larger (Fig. 4B,B′). The aspect ratio of cells in the border region (II) was the highest (average 3.13) (Fig. 4C′, region II) whereas other regions were comparable (average 1.56) (Fig. 4C,C′).

DISCUSSION

We used a series of reporter mouse lines expressing fluorescent proteins, in combination with image analysis methods, to investigate the trends in global cellular behaviors of VE cells throughout gastrulation. *R26R-ManGeKyou* mice exhibited ubiquitous expression of fluorescent proteins during development, as expected; however, for reasons yet to be determined, mKeima-Red was not detectable. There are several possible explanations for this observation. We tested several combinations of excitation wavelengths and filter sets; it may be that the expression level of mKeima-Red is simply insufficient for detection. We also examined other tissues in late-stage embryos, but could not observe Keima-Red signals at any stage, suggesting that weak promoter activity is a less likely explanation for the lack of detection of Keima-Red signal. Alternatively, recombination may not be performed properly, causing the allele that expresses mKeima-Red to be generated only infrequently.

Our novel image-analysis method, LP-Clonal, allows quantification of cluster shapes. LP-Clonal can be adapted for shape analyses in various tissues and experimental organisms, including zebrafish, fruit fly, and plant (Weissman and Pan, 2015). Multicolor lineage labeling combined with quantitative image analysis will provide a deeper understanding of common rules of cell behaviors in embryogenesis and organogenesis.

The directional bias of cell-cluster shape may reflect the axis of tissue expansion caused by directional cell divisions. During time-lapse imaging, the ExEmVE cells were not intermingled during recording, and daughter cells were positioned along the anterior-proximal to posterior-medial direction. Observations over a long period of lineage tracking were in agreement with time-lapse recordings, confirming the presence of large, elongated clusters with the same origin. These results suggest that ExEmVE cells are tightly packed and less motile. The stripes observed near the border

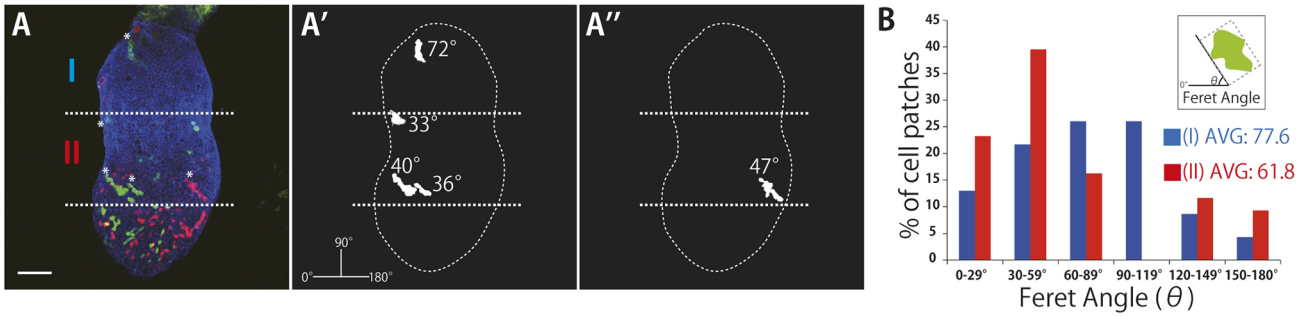

Fig. 3. Distribution of cell descendants labeled during early post-implantation. (A) Examples of *z*-stack images of E7.5 *R26R-MGK*/*R26CreER* embryos treated with tamoxifen at E5.5. White asterisks indicate analyzed cell clusters consisting of more than two cells. Regions I and II represent the proximal and the middle portions of embyros, respectively. (A′,A″) Binary images used for image analysis. The Feret angles of cell clusters are shown. (B) Frequency distribution of patches within given ranges of angles among 31 images. Regions I and II comprise 23 and 43 patches, respectively. *x*- and *y*-axes indicate frequency of analyzed patches and angle ranges, respectively. Green, red and blue indicate EGFP, mCherry and CF405 phalloidin fluorescence, respectively. Scale bar: 100 µm.

Development (2018) 145, dev165852. doi:10.1242/dev.165852

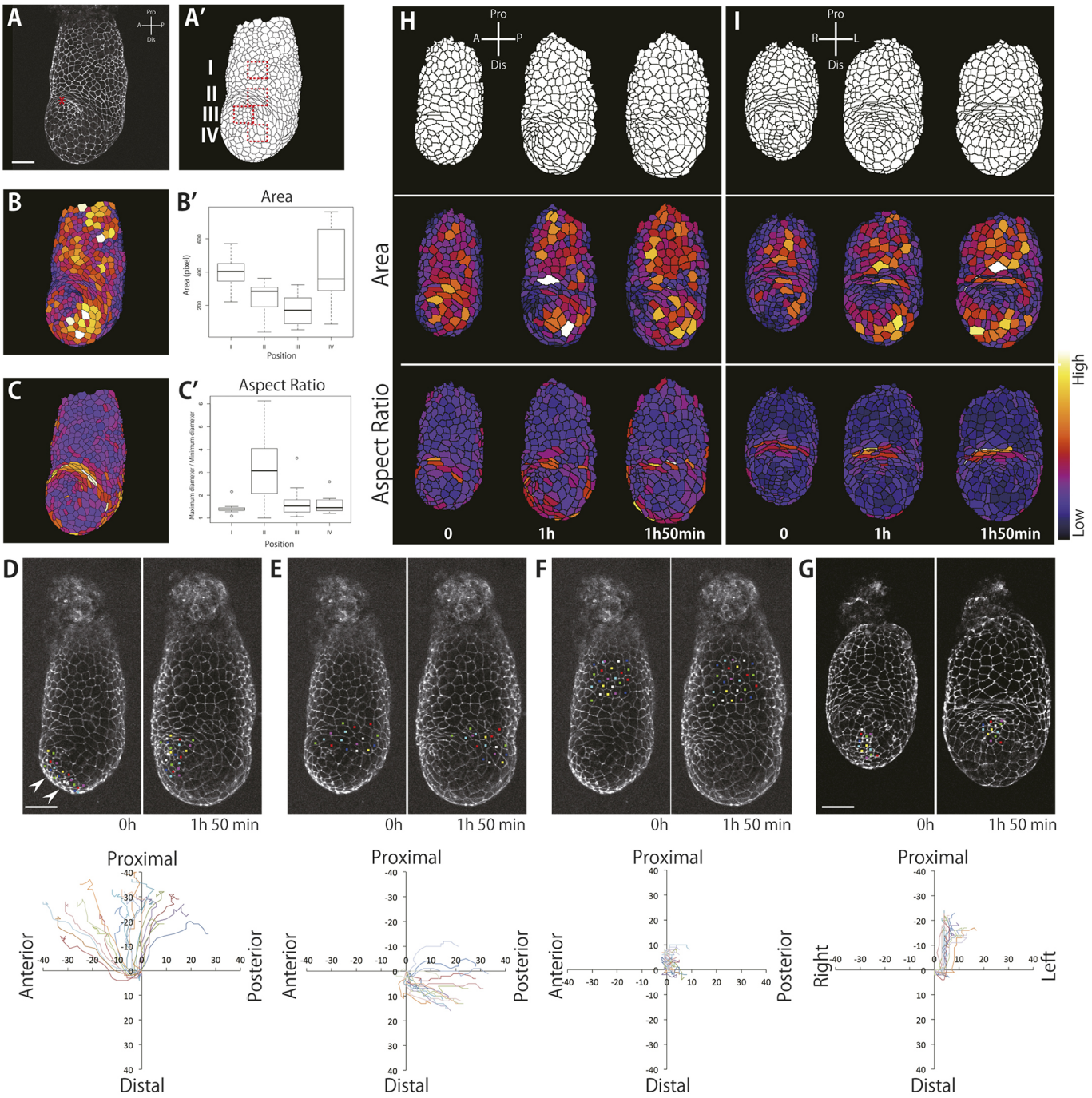

Fig. 4. Quantification of cell shape and positional changes in the embryonic visceral endoderm. (A) Image of a *R26-PHA7-EGFP* embryo at around E6.5. Embryos are observed from anterior (indicated with red asterisk) to lateral. (A′) The binary image of the embryo shown in A. Boxed areas are applied for image analysis. (B,C) Heat maps of quantified areas (B) and aspect ratios (C). (B′,C′) Box plots of the quantified data shown in B and C, respectively. The box and whiskers indicate interquartile ranges and extreme values, respectively. (D-G) Snapshot images of time-lapse recordings of E6.25 *R26-PHA7-EGFP* embryos at 0 and 1 h 50 min. Colored dots indicate the tracked cells and the trajectories are shown in the graphs below. Arrowheads indicate migrating cells. (H,I) Results of quantitative analyses of the embryos shown in D-F (H) and G (I); surface areas and aspect ratios are shown as heat maps. A, anterior; Dis, distal; L, left; P, posterior; Pro, proximal; R, right. Scale bars: 50 µm.

between Em and ExEm regions suggest that these two regions are strictly compartmentalized. When the original AVE cells start to move, the ExEmVE cells are tightly packed with enrichment of F-actin and myosin IIA in the apical cell cortex in ExEmVE cells (Trichas et al., 2011), but not in EmVE cells. This may inhibit ExEmVE cells from moving actively, leading to large clusters of cells, and may provide a physical barrier that prevents EmVE cells from migrating across the Em region, especially AVE cells. By contrast, cells in the EmVE layer did not form any coherent cluster, and active cell movements were observed. This may be correlated with the intercalation of epiblast-derived definitive endoderm cells (Kwon et al., 2008; Viotti et al., 2014).

Development (2018) 145, dev165852. doi:10.1242/dev.165852

This study suggests that VE cells show differential cell behaviors depending on the region even after the original AVE migration, a key event underlying the establishment of the A-P axis. Our study indicates that the global cell behavior of the VE is maintained even after AVE migration, and that this global cell behavior may be important for changes in the embryo's global morphology around this stage. These region-specific behaviors may correlate with morphological changes of other layers, namely the epiblast, extra-embryonic ectoderm, and mesoderm. These behaviors can be elucidated by modifying cellular behaviors in a region- and layer-specific manner.

MATERIALS AND METHODS

Mouse strains

R26R-ManGeKyou (*R26R-MGK*) (accession number CDB0222K) and *R26R-EGFP* (accession number CDB0297K) mice were established following the strategy described previously (Abe et al., 2011). *R26R-MGK*-targeting vector was constructed using the p*BigT* plasmid as starting material (Srinivas et al., 2001). cDNAs encoding fluorescent proteins for mKeima-Red, EGFP and mCherry were derived from p*mKeima-Red-S1* (MBL), p*EGFP* and p*mCherry* (Shaner et al., 2004), respectively. Annealed oligonucleotides were used to insert *lox2272* and *lox5171* sites behind splicing acceptor (SA) in *pBigT*. The modified *BigT*, *SA/lox5171/lox2272/loxP/PGK-Neo-triple SV40 pA (STOP)/mKeima-Red-bpA-lox12-EGFP-bpA-lox2272-mCherry-bpA*, was inserted into p*MC1-DT-A-Rosa26* (Abe et al., 2011; Yagi et al., 1993a). To generate the targeting vectors *R26R-EGFP*, the cDNAs for *EGFP* was cloned into p*ENTR2B* and subsequently re-cloned into the *Rosa26-STOP*-targeting vector (Abe et al., 2011). *R26R-MGK*-targeting vectors were introduced into *TT2* ESCs derived from an F1 hybrid embryo between C57BL/6 and CBA mice (Yagi et al., 1993b), and *R26R-EGFP*-targeting vectors were introduced into HK3i ESCs of an inbred C57BL/6 background (Kiyonari et al., 2010). Homologous recombinant ESCs were isolated, and chimeric mice were generated according to standard procedures. Offspring were routinely genotyped by PCR as described (Abe et al., 2011). The *R26R-MGK* and *R26R-EGFP* mice were bred to homozygosity; homozygous mice were viable and fertile, and exhibited no obvious phenotypes. Further details concerning reporter mouse production will be provided upon request (http://www2.clst.riken.jp/arg/reporter_mice.html).

R26CreER (B6;129-Gt(ROSA)26Sor$^{tm1(cre/Esr1)Nat}$*/J)* (Badea et al., 2003) and *EIIa-Cre (C5379Lmgd/J B6.FVB-Tg(EIIa-cre)C5379Lmgd/J)* (Lakso et al., 1996) were obtained from the Jackson Laboratory, and *R26-PHA7-EGFP* (accession number CDB0261K) was established previously (Shioi et al., 2017). All animal experiments were approved by the Institutional Animal Care and Use Committee of RIKEN Kobe Branch and performed according to RIKEN animal experimentation guidelines.

In vitro Cre recombination

R26R-MGK ESCs were transiently transfected with the p*Cre-Pac* plasmid and selected with puromycin (1 µg/ml) for 24 h (Taniguchi et al., 1997). After the treatment, cells were fixed in 4% paraformaldehyde (PFA) for 30 min, washed three times with PBS, and stained with DAPI.

Mouse embryo preparation

R26R-MGK mice were crossed with *EIIaCre* to obtain two-cell-stage and E7.5 embryos that express fluorescent probes randomly. To enable temporal induction of recombination, *R26R-MGK* and *R26R-EGFP* mice were mated with *R26CreER* mice. Tamoxifen was dissolved in sunflower seed oil to 10 mg/ml concentration, and injected intraperitoneally into pregnant females at E5.5 at a dose of 0.5 mg/25 g. *R26-PHA7-EGFP* mice were crossed with wild-type C57BL/6. The embryos were dissected in ice-cold DMEM without Phenol Red and fixed with 4% PFA. After rinsing three times with PBS, they were stained with phalloidin (CF405 Phalloidin, Biotium) or DAPI at 4°C overnight.

Imaging of embryos

Fixed samples were imaged with an A1-Ti confocal microscope (Nikon), or a Macro Confocal Laser Microscope System AZ-C1 (Nikon). The time-lapse recording of two-cell-stage *EIIaCre/R26R-MGK* embryos and E6.5 *R26CreER/R26R-EGFP* embryos were performed with the Olympus incubation imaging system LCV100 [CSU10 (Yokogawa), iXon+EMCCD (Andor)]. For *R26-PHA7-EGFP* embryos, we used an A1-Ti confocal microscope with an incubation culture system (TOKKEN). Pre-implantation stage embryos were cultured in KSOM, and post-implantation stage (E6.25 onwards) embryos were embedded in collagen gel (Nitta Gelatin) containing DMEM and supplemented with 50% rat serum as described (Abe et al., 2013a). Cell tracking was performed with the manual tracking plug-in for ImageJ. *xy* coordinates and calculations were generated in using Excel.

Quantitative analyses of embryo images

z-stacks of embryos were obtained as described above, and the images were transformed with the anterior side to the left. For quantifying tilting angle of clusters in the E7.5 *EIIaCre/R26R-MGK* embryo using LP-Clonal plug-in (https://lpixel.net/en/products/lp-series/lp-clonal/), the acquired images were converted to maximum-intensity-projected (MIP) images and the shapes of the embryo region were normalized using the NormalizeShape function as described in Results. Binary images were generated from the normalized MIP images to mark the cluster regions as masked. The LP-Clonal plugin internally split the binary images into square subregions with dimensions of 100×100 pixels. Each subregion was subsequently transformed into 2D autocorrelation spectra, also with dimensions of 100×100 pixels, to calculate the angles and aspect ratios in observed cluster regions. The angle of each cluster region was determined by identifying the pixel with maximum intensity (M) from the pixels on a circular perimeter (5-pixel diameter). The vector of the center pixel of the 2D autocorrelation spectrum to the identified maximum-intensity pixel on the perimeter represents the tilt angle of the cluster region. The aspect ratio of the cluster region was measured by an approximated ellipse derived from an iso-contour with intensity M. When growth direction is sharp, the aspect ratio is low and the contour is thin. By contrast, when the growth of clonal cells is spatially uniform, the aspect ratio is high and the contour has a circular shape. As a post-processing analysis step, we averaged the tilt angles and aspect ratios for each subregion. To quantify the angles between the maximum caliper and the surface area of cell patches in E7.5 *R26CreER/R26R-MGK* embryos, we used BioVoxxel_Toolbox (http://imagej.net/BioVoxxel_Toolbox). Binary images were made with the projected images from each channel, converted to mask (size: 0-500), removing noise signals derived from fewer than two cells. To estimate the cell number within a patch, the minimum value of an area containing two cells was set to 2.0, and the ratios of the minimum value (corresponding to a single cell) to a patch area were calculated for each patch.

For analyzing cell morphologies in *R26-PHA7-EGFP* embryos, BioVoxxel Toolbox was used. The noise signals inside the VE layer in each image were manually removed by ImageJ (Fig. 4A: 1024×1024; Fig. 4D, E: 512×512). The binary images were created by the projected images and skeletonized. The skeletonized images were reprocessed manually using Adobe Photoshop according to the original projected images, and the finalized images were analyzed by Shape Descriptor Maps (BioVoxxel Toolbox). This returned the value of cell surface and aspect ratio (AR=maximum caliper diameter/minimum caliper diameter). The resultant values from these image analyses were plotted with RStudio software.

Acknowledgements

We thank Dr Shankar Srinivas for the gift of the p*BigT* plasmid, the late Dr Roger Y. Tsien for the mCherry plasmid, Dr Jan Brocher for the BioVoxxel ToolBox, and Dr Takeshi Yagi for the Cre-Pac plasmid. We are also indebted to members of the Laboratories for Animal Resource Development and Genetic Engineering at the RIKEN Center for Biosystems Dynamic Research for skillful technical assistance and dedicated support in generating reporter mice and in housing animals.

Competing interests

The authors declare no competing or financial interests.

Author contributions

Conceptualization: T.A., T.F.; Methodology: T.A., T.F.; Software: N.K.; Validation: T.A., T.F.; Formal analysis: T.A.; Investigation: T.A.; Resources: H.K.; Data curation:

T.A.; Writing - original draft: T.A., T.F.; Writing - review & editing: T.A., Y.F., T.F.; Visualization: T.A.; Supervision: T.F.; Project administration: Y.F.; Funding acquisition: T.A., N.K., H.K., Y.F., T.F.

Funding

This work was supported by intramural grants from RIKEN and Japan Society for the Promotion of Science KAKENHI (JP16K19042, JP17H03689 and JP16K18562). T.F. was supported by Japan Science and Technology Agency, Core Research for Evolutional Science and Technology (JPMJCR1654) and Ministry of Education, Culture, Sports, Science and Technology [KAKENHI 16H06280 (ABiS)].

Supplementary information

Supplementary information available online at
http://dev.biologists.org/lookup/doi/10.1242/dev.165852.supplemental

References

Abe, T., Kiyonari, H., Shioi, G., Inoue, K.-I., Nakao, K., Aizawa, S. and Fujimori, T. (2011). Establishment of conditional reporter mouse lines at ROSA26 locus for live cell imaging. *Genesis* **49**, 579-590.

Abe, T., Aizawa, S. and Fujimori, T. (2013a). Live imaging of early mouse embryos using fluorescently labeled transgenic mice. *Methods Mol. Biol.* **1052**, 101-108.

Abe, T., Sakaue-Sawano, A., Kiyonari, H., Shioi, G., Inoue, K.-I., Horiuchi, T., Nakao, K., Miyawaki, A., Aizawa, S. and Fujimori, T. (2013b). Visualization of cell cycle in mouse embryos with Fucci2 reporter directed by Rosa26 promoter. *Development* **140**, 237-246.

Badea, T. C., Wang, Y. and Nathans, J. (2003). A noninvasive genetic/pharmacologic strategy for visualizing cell morphology and clonal relationships in the mouse. *J. Neurosci.* **23**, 2314-2322.

Beddington, R. S. P. and Robertson, E. J. (1999). Axis development and early asymmetry in mammals. *Cell* **96**, 195-209.

Fujimori, T., Kurotaki, Y., Miyazaki, J.-I. and Nabeshima, Y.-I. (2003). Analysis of cell lineage in two- and four-cell mouse embryos. *Development* **130**, 5113-5122.

Gardner, R. L. and Cockroft, D. L. (1998). Complete dissipation of coherent clonal growth occurs before gastrulation in mouse epiblast. *Development* **125**, 2397-2402.

Ghigo, C., Mondor, I., Jorquera, A., Nowak, J., Wienert, S., Zahner, S. P., Clausen, B. E., Luche, H., Malissen, B., Klauschen, F. et al. (2013). Multicolor fate mapping of Langerhans cell homeostasis. *J. Exp. Med.* **210**, 1657-1664.

Griswold, S. L., Sajja, K. C., Jang, C.-W. and Behringer, R. R. (2011). Generation and characterization of iUBC-KikGR photoconvertible transgenic mice for live time-lapse imaging during development. *Genesis* **49**, 591-598.

Holzenberger, M., Lenzner, C., Leneuve, P., Zaoui, R., Hamard, G., Vaulont, S. and Bouc, Y. L. (2000). Cre-mediated germline mosaicism: a method allowing rapid generation of several alleles of a target gene. *Nucleic Acids Res.* **28**, e92.

Kiyonari, H., Kaneko, M., Abe, S.-I. and Aizawa, S. (2010). Three inhibitors of FGF receptor, ERK, and GSK3 establishes germline-competent embryonic stem cells of C57BL/6N mouse strain with high efficiency and stability. *Genesis* **48**, 317-327.

Kwon, G. S., Viotti, M. and Hadjantonakis, A.-K. (2008). The endoderm of the mouse embryo arises by dynamic widespread intercalation of embryonic and extraembryonic lineages. *Dev. Cell* **15**, 509-520.

Lakso, M., Pichel, J. G., Gorman, J. R., Sauer, B., Okamoto, Y., Lee, E., Alt, F. W. and Westphal, H. (1996). Efficient in vivo manipulation of mouse genomic sequences at the zygote stage. *Proc. Natl. Acad. Sci. USA* **93**, 5860-5865.

Lawson, K. A. and Pedersen, R. A. (1987). Cell fate, morphogenetic movement and population kinetics of embryonic endoderm at the time of germ layer formation in the mouse. *Development* **101**, 627-652.

Lee, G. and Saito, I. (1998). Role of nucleotide sequences of loxP spacer region in Cre-mediated recombination. *Gene* **216**, 55-65.

Livet, J., Weissman, T. A., Kang, H., Draft, R. W., Lu, J., Bennis, R. A., Sanes, J. R. and Lichtman, J. W. (2007). Transgenic strategies for combinatorial expression of fluorescent proteins in the nervous system. *Nature* **450**, 56-62.

Meng, W., Mushika, Y., Ichii, T. and Takeichi, M. (2008). Anchorage of microtubule minus ends to adherens junctions regulates epithelial cell-cell contacts. *Cell* **135**, 948-959.

Rossant, J. and Tam, P. P. L. (2009). Blastocyst lineage formation, early embryonic asymmetries and axis patterning in the mouse. *Development* **136**, 701-713.

Schäfer, I., Müller, C., Luhmann, H. J. and White, R. (2016). MOBP levels are regulated by Fyn kinase and affect the morphological differentiation of oligodendrocytes. *J. Cell Sci.* **129**, 930-942.

Shaner, N. C., Campbell, R. E., Steinbach, P. A., Giepmans, B. N. G., Palmer, A. E. and Tsien, R. Y. (2004). Improved monomeric red, orange and yellow fluorescent proteins derived from Discosoma sp. red fluorescent protein. *Nat. Biotechnol.* **22**, 1567-1572.

Shioi, G., Hoshino, H., Abe, T., Kiyonari, H., Nakao, K., Meng, W., Furuta, Y., Fujimori, T. and Aizawa, S. (2017). Apical constriction in distal visceral endoderm cells initiates global, collective cell rearrangement in embryonic visceral endoderm to form anterior visceral endoderm. *Dev. Biol.* **429**, 20-30.

Snippert, H. J., van der Flier, L. G., Sato, T., van Es, J. H., van den Born, M., Kroon-Veenboer, C., Barker, N., Klein, A. M., van Rheenen, J., Simons, B. D. et al. (2010). Intestinal crypt homeostasis results from neutral competition between symmetrically dividing Lgr5 stem cells. *Cell* **143**, 134-144.

Soriano, P. (1999). Generalized lacZ expression with the ROSA26 Cre reporter strain. *Nat. Genet.* **21**, 70-71.

Srinivas, S. (2006). The anterior visceral endoderm-turning heads. *Genesis* **44**, 565-572.

Srinivas, S., Watanabe, T., Lin, C.-S., William, C. M., Tanabe, Y., Jessell, T. M. and Costantini, F. (2001). Cre reporter strains produced by targeted insertion of EYFP and ECFP into the ROSA26 locus. *BMC Dev. Biol.* **1**, 4.

Srinivas, S., Rodriguez, T., Clements, M., Smith, J. C. and Beddington, R. S. P. (2004). Active cell migration drives the unilateral movements of the anterior visceral endoderm. *Development* **131**, 1157-1164.

Tabansky, I., Lenarcic, A., Draft, R. W., Loulier, K., Keskin, D. B., Rosains, J., Rivera-Feliciano, J., Lichtman, J. W., Livet, J., Stern, J. N. H. et al. (2013). Developmental bias in cleavage-stage mouse blastomeres. *Curr. Biol.* **23**, 21-31.

Takaoka, K., Yamamoto, M. and Hamada, H. (2011). Origin and role of distal visceral endoderm, a group of cells that determines anterior-posterior polarity of the mouse embryo. *Nat. Cell Biol.* **13**, 743-752.

Tam, P. P. L. and Loebel, D. A. F. (2007). Gene function in mouse embryogenesis: get set for gastrulation. *Nat. Rev. Genet.* **8**, 368-381.

Taniguchi, M., Yuasa, S., Fujisawa, H., Naruse, I., Saga, S., Mishina, M. and Yagi, T. (1997). Disruption of semaphorin III/D gene causes severe abnormality in peripheral nerve projection. *Neuron* **19**, 519-530.

Trichas, G., Joyce, B., Crompton, L. A., Wilkins, V., Clements, M., Tada, M., Rodriguez, T. A. and Srinivas, S. (2011). Nodal dependent differential localisation of dishevelled-2 demarcates regions of differing cell behaviour in the visceral endoderm. *PLoS Biol.* **9**, e1001019.

Tzouanacou, E., Wegener, A., Wymeersch, F. J., Wilson, V. and Nicolas, J.-F. (2009). Redefining the progression of lineage segregations during mammalian embryogenesis by clonal analysis. *Dev. Cell* **17**, 365-376.

Viotti, M., Nowotschin, S. and Hadjantonakis, A.-K. (2014). SOX17 links gut endoderm morphogenesis and germ layer segregation. *Nat. Cell Biol.* **16**, 1146-1156.

Weber, R. J., Pedersen, R. A., Wianny, F., Evans, M. J. and Zernicka-Goetz, M. (1999). Polarity of the mouse embryo is anticipated before implantation. *Development* **126**, 5591-5598.

Weissman, T. A. and Pan, Y. A. (2015). Brainbow: new resources and emerging biological applications for multicolor genetic labeling and analysis. *Genetics* **199**, 293-306.

Yagi, T., Nada, S., Watanabe, N., Tamemoto, H., Kohmura, N., Ikawa, Y. and Aizawa, S. (1993a). A novel negative selection for homologous recombinants using diphtheria toxin A fragment gene. *Anal. Biochem.* **214**, 77-86.

Yagi, T., Tokunaga, T., Furuta, Y., Nada, S., Yoshida, M., Tsukada, T., Saga, Y., Takeda, N., Ikawa, Y. and Aizawa, S. (1993b). A novel ES cell line, TT2, with high germline-differentiating potency. *Anal. Biochem.* **214**, 70-76.